

An Approach for Fan Stage Conceptual Design with Non-Axisymmetric Stators in Presence of Distortion

Manish Pokhrel*, Jonathan Gladin†
Russell K. Denney † Dimitri N. Mavris‡

*Daniel Guggenheim School of Aerospace Engineering,
Georgia Institute of Technology, Atlanta, Georgia, 30332*

Advances in the study of distortion warrant the consideration of non-axisymmetric flow field impacts on fan designs. The lack of a method that considers such impacts in early design motivates this work. An approach to design a fan stage in the presence of distortion is developed and illustrated here. In the proposed approach, an extension of the multi-meanline method accounts for flow asymmetry. Blade metal angles for the rotor are designed considering minimization of overall rotor losses in presence of incidence swings. Corrections to the quasi-steady rotor exit conditions provide an approximation to the unsteady rotor response. Non-axisymmetric stators are designed to reduce stage losses. The concept of Multi-Design Point (MDP) approach in the thermodynamic cycle designs inspires this work. This approach is envisioned as a method to approximate the design point of a fan stage under distorted flow conditions.

I. Introduction

The first component of turbomachinery that the flow encounters is the fan. For under-wing engine applications, the flow that the fan sees can be treated as uniform for conceptual level modeling. However, when operating under distorted inflow, as in boundary layer ingestion (BLI), this assumption is not valid anymore due to the inherent flow distortion that arises from ingesting the boundary layer. The design of a rotor should not be treated independently for BLI applications. It is a highly coupled inlet-rotor-stator design problem. The goal is to design an inlet and a fan stage that is able to perform in the harsh conditions created by the boundary layer flow. The inlet should be designed such that it maximizes the pressure recovery and that the fan can sustain the level of incoming swirl and total pressure distortion both aerodynamically and structurally. In this work, the rotor-stator portion of the problem is considered under the assumption that the flow at the rotor inlet is known.

The rotor experiences spatial and temporal variation in the flow field that need to be considered. Treating the flow as uniform shall likely misrepresent the actual performance and also yield a non-optimum fan stage. For the design of fans operating in a distorted flow field, few challenges arise. The first challenge is to minimize the rotor losses in presence of distortion. Rotor unsteady response is generally ignored in conceptual turbomachinery design. Since unsteadiness is inherent in distorted flow conditions, it is important to understand if rotor unsteady response needs to be modeled for specific distortion conditions. Non-axisymmetric stators have shown to reduce stator losses in BLI flow field, but an approach to be used in the conceptual design phase is lacking. Maintaining a required pressure rise in the presence of non-uniformities also another challenge. This paper attempts to resolve these challenges. In addition, it also aims to bring all these elements together to create a design optimization framework.

In the subsequent sections, an overview of literature is presented first. The methodology section will describe the development of the proposed framework. The setup of test cases is described next. The analysis of several elements of the design framework are presented in the results section. The analysis on

*PhD Candidate, Aerospace Systems Design Laboratory, AIAA Student Member

†Research Engineer II, Aerospace Systems Design Laboratory, AIAA Member

‡S.P. Langley Distinguished Regents Professor, Aerospace Systems Design Laboratory, AIAA Fellow

contributions of each modeling element to the final design is discussed, following which the results of the optimization of high level design variables are presented. The final section summarizes the major points of this work.

II. Literature

Fig. 1 represents the iteration that occurs between cycle design and fan design. Initially, a cycle designer may choose to use some representative map and perform the first iteration of cycle design. Stage requirement is set that leads to fan design, which then produces an updated version of the fan map. The fan is designed for the flow profile determined by the inlet at the Aerodynamic Interface Plane (AIP). If the designed fan cannot sustain the level of incoming swirl and pressure distortion, the inlet needs to be redesigned such that the flow at the fan face is not too severe for the operability of the propulsor. The inlet performance is also supplied to the cycle design so that an accurate estimate of the flow being ingested is passed on to the cycle analysis/design. NASA Inlet A is an example of an inlet design that is designed for the purposes of distortion.

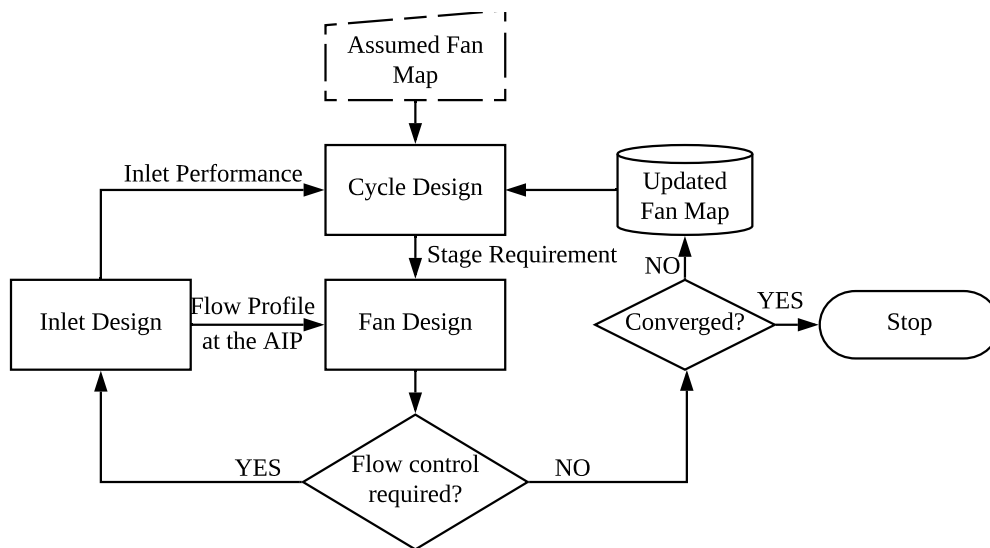


Figure 1. Iteration among inlet design, cycle design, and component design.

A fan stage that is not designed for distortion purposes departs from its normal operating condition when operating in a distorted inflow. Swirl and total pressure distortion lead to incidence angle variations on the fan. In the hub region, due to more mass flow redistribution, the axial velocity distortion is attenuated compared to the inlet entrance; however, the spinning of the hub creates more swirl distortion. So, swirl distortion is mainly responsible for large incidence variations on the fan at the hub region. Near the tips, the total pressure distortion is more dominant than swirl distortion and that creates a large axial velocity non-uniformity, which is responsible for incidence swings. Both swirl and total pressure distortion translate into incidence variations for the fan. Swirl angle, axial velocity, and the blade metal angle at the leading edge combined determine the incidence angle for the blade. Fig. 2 provides a schematic description of the incidence angle, blade leading edge angle, stagger angle (γ), relevant relative (W) and absolute (C) flow velocities, and blade speed (U).

Fig. 3 illustrates the isolated effects of swirl and total pressure distortion on velocity triangles and consequently, on the incidence angles. C is the absolute velocity, C_a is the axial velocity, W is the relative velocity, and U is the blade speed. α and β are the absolute and relative flow angles respectively.

In an integrated inlet/rotor design process conducted by UTRC under the BLI2DTF group,¹ several iterations between inlet and rotor design led to the final design of inlet and the fan. The inlet design started with Inlet A and it was observed that the distortion created by the inlet was not aeromechanically sustainable for the fan. The incidence swing was around 17° and swirl angle distribution ranged from $+16^\circ$ to -24° . These large variations in incidence swings lead to losses in the rotor. The blade was modified to minimize the losses using results from 3-D analysis and heuristic expertise.

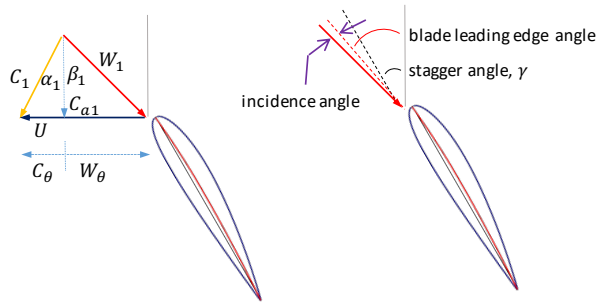


Figure 2. Dependence of incidence angle on axial velocity and swirl angle.

A fan is designed to raise the pressure of a given mass of fluid to a certain level in addition to achieving an adequate stall margin available and peak efficiency at design point.² The energy corresponding to the change in pressure is due to the energy imparted by the rotor to the flow. Fan conceptual design comprises of computing the flow angles, blade angles, their radial variation, twist, and basic airfoil geometry description.

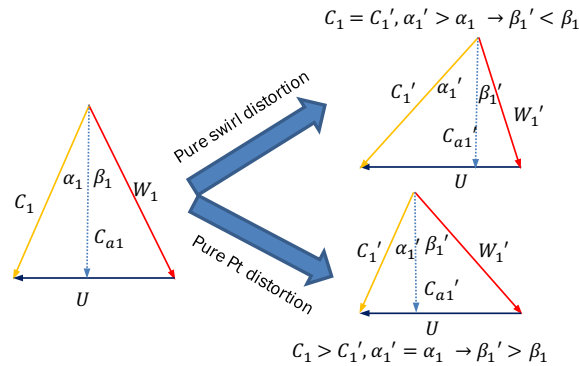


Figure 3. Effect of pure swirl and total pressure distortion on velocity triangles.

The process begins with the mean line design. At this stage, the annulus is defined and the calculations are performed between the blade rows along the mean radius. The calculations are 1-D and the flow is assumed to be inviscid. Viscous and 3-D effects are included in the form of empirical loss models. In the multi-meanline design, the radial variation of the flow is also considered, so the spanwise velocity triangles determine the twist of the blades. Radial equilibrium is employed which basically ensures the balance of the radial pressure of the flow and the centripetal force of the rotating flow. Multi-meanline still assumes some airfoil profile and uses empirical correlations for loss models. Meanline and multi-meanline methods are generally regarded as the conceptual design tools for the compressor. A review of conceptual design tools for turbomachinery design does not provide any direct way of handling distorted inflow and minimizing these losses.

These conceptual tools, in addition, also compute the quasi-steady flow at the rotor exit. Steady computations assume that the blade responds instantaneously to the changing flow conditions at its given operating condition. If not, then the quasi-steady response has to be corrected to account for the unsteady departure. The flow in a turbomachine is fundamentally unsteady. Dean³ first showed that for a turbine or a compressor to provide shaft work or absorb the work, there must exist local unsteady changes in static pressure. Although the flow is unsteady in an absolute frame of reference, it is possible to treat the flow as steady by using Euler turbomachinery equation in the relative frame of reference.⁴ If a turbomachine includes only one blade, the flow is uniform, and relative frame of reference is used, then the problem can be treated as steady by writing the governing equations accordingly.⁵ In this paper, unsteadiness in turbomachinery refers to the additional periodic unsteadiness due to distortion and not the inherent unsteadiness that exist in all kinds of flows.

In reality, the interaction of rotor with the non-uniform flow field results in an unsteady rotor response. Methods for distortion analysis like parallel compressor theory⁶ and actuator disk⁷ assume that the rotor response is instantaneous. Cousins⁸ identified that the unsteadiness of the rotor blade is a function of the blading itself and that has to do with the time the blade takes to respond to the instantaneous flow conditions. While most distortion studies assume quasi-steady response, it becomes important to understand the consequence of not modeling unsteadiness in the conceptual design.

Carta⁹ and Bielewa¹⁰ developed a synthesis method that can isolate the non-linear dynamic contributions to the airloads by subtracting the static coefficients from the total airloads.¹¹ Carta⁹ used this idea to compute the unsteady rotor performance given the given the knowledge of the quasi-steady rotor, steady airfoil, and unsteady airfoil performances. This method is also in philosophical agreement with the work of Cousins.⁸ However, this method has not been used in the design process yet. This study will aim to utilize this method in the design process and estimate the effects of additional unsteady contribution.

The flow exiting the rotor is also non-uniform. Conventional stator rows are not designed for circumferentially varying flow in terms of swirl, radial angle, and most importantly, the mass flux. Low axial velocity regions at the rotor exit result in a shorter vector of the relative velocity. When converted into the absolute frame, this vector is overturned. This results in a positive incidence and consequently, increases the turning requirement in the stator. It is known that reducing the diffusion factor at the exit directly correlates to increasing the stage efficiency. These flow angle variations at stator inlet leads to increased losses in axisymmetric stator. Some higher fidelity studies^{12,13} have shown that non-axisymmetric stator reduces the losses in the stage and is a better option for fans subjected to non-uniform flows. The conclusions showed by these studies highlight promising results of the non-axisymmetric stator design. Performing the design changes during CFD means that most design parameters are already fixed and other stage parameters are not optimized for the stator design changes, Bringing this in the conceptual design phase has two advantages: (i) more accurate representation of fan maps for conceptual design trade studies, and (ii) better fan stage performance due to the freedom of other design variables to vary simultaneously with the stator design changes. The methodology section will discuss the proposed framework for designing the fan stage in conceptual phase considering several aspects discussed above - flow asymmetry, rotor loss minimization, unsteady rotor response, and non-axisymmetric stator design. Using this framework, the high level variables of the fan stage will be varied to explore the design space with the goal of achieving maximum stage efficiency subject to the satisfaction of other aerodynamic constraints.

III. Methodology

The design of a fan stage can be split into several modeling elements. To understand the modeling elements, it is convenient to follow the flow through the fan stage. The process comprises the following elements:

1. Rotor design considering asymmetric flow
2. Unsteady rotor response from quasisteady response
3. Non-axisymmetric stator design
4. Loop to vary the rotor design in 1 until target pressure rise is achieved

Below, a brief descriptions to each step is given. As mentioned earlier, it is assumed that the flow profile information at the AIP is known. The discussed methodology is implemented on the platform of NASA's OTAC (Object Oriented Turbomachinery Analysis Code) tool¹⁴ leveraging its already existing meanline modeling capabilities.

A. Rotor design

The losses in the rotor become more pronounced when operating in a distorted flow field. Therefore, it is important to come up with a design that can minimize the losses in the rotor. Designing the rotor for distortion purposes, therefore, means minimizing overall losses.

While the losses are a result of various 3-D effects of the flow, in conceptual design, empirical loss relations are added in order to describe and include the losses occurring in the compressor. The loss models used

by turbomachinery companies are proprietary in nature. There are several loss models available in the literature.¹⁵⁻¹⁹ All these loss models typically constitute a loss in total pressure and are used in the form of coefficients. Eq. 1 shows the form of loss coefficient, where 1 is the inlet, 2 is the exit, and ' refers to an isentropic process.

$$\bar{\omega}_r = \frac{P_{t2',rel} - P_{t2,rel}}{P_{t1,rel} - P_{s1}} \quad (1)$$

The majority of the losses in subsonic cascades come from the profile loss. Shock losses and endwall losses are almost negligible compared to the profile loss. For the purposes of this study, only profile losses are investigated, and losses are mass-averaged in case of non-uniform flows.

The modeling technique gets some inspiration from the Multi-Design Point (MDP) approach used in the engine modeling side. Traditionally, an engine is designed at a design point (usually cruise or sea level condition). When the engine has been optimized to work for cruise condition, some off-design constraints are checked (for example: climb condition and sea level thrust). When these constraints are met, the engine is considered to be optimal. However, an ideal condition would be to design an engine that provides an optimal performance throughout the mission. Plus, it might be optimal to meet some equality constraints on off-design. That means, a single design point is not necessarily the correct approach to design engines under these conditions. MDP method allows to vary engine parameters in the design point such that the off-design constraints are automatically ensured. While not exactly the same approach, the modeling technique being employed here for rotor design is something similar.

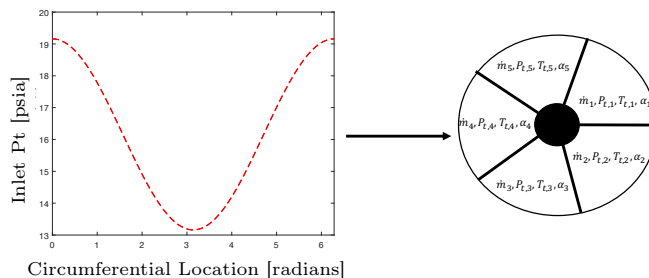


Figure 4. Representation of continuous flow profile via discrete uniform sectors..

Let's say, a non-uniform flow field at the AIP is given. A simplification is made here: the smooth non-uniformity in the flow field is discretized into circumferential sectors of uniform flow as shown in Fig. 4. In the example shown, the smooth total pressure profile is used to locate five sectors. The goal is to design a rotor blade with an overall peak operating efficiency when operating in these discretized sectors.

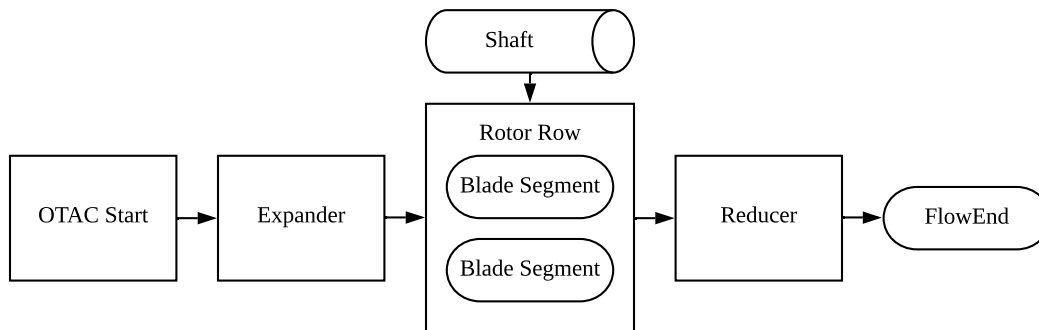


Figure 5. Schematic representing rotor design/analysis assembly.

First, a rotor modeling assembly (Fig. 5) is created that can operate in both "design" and "off-design" conditions. When run in design mode, the blade angles are computed to ensure the enthalpy rise (or any other similar target parameter) such that the incidence and deviation are equal to the design values supplied and when run in off-design mode, the saved geometry from the design mode will calculate the enthalpy rise and the rotor losses. A conventional multi-meanline modeling technique that uses some uniform flow

condition is used to design the rotor. This designed rotor has to operate in the conditions of asymmetric flow field (the discretized sectors, as mentioned above).

For this proposed framework, the rotor is designed for some uniform flow. That means, the design point flow needs to account for the non-uniformities present in the true operating condition (like the one shown in Fig. 4. Understanding that the "design" point is not the true operating point allows to intentionally produce a non-optimal rotor in the design point, but the one that has minimal losses when operating in off-design points. This philosophy has been used in the framework shown in Fig. 6.

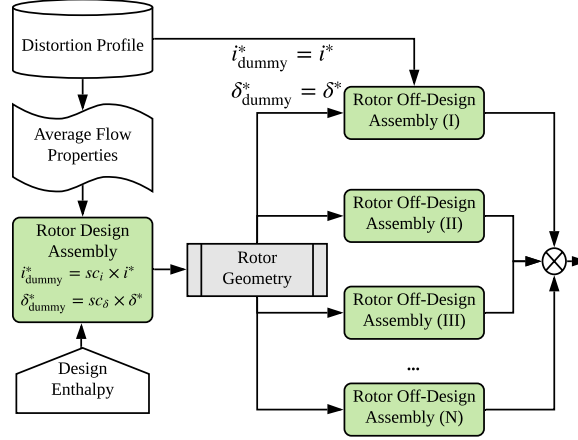


Figure 6. Rotor design framework.

First, a design point assembly of the rotor is used to design the rotor for mass-averaged flow. Each rotor design/off-design box includes a rotor assembly like the one shown in Fig. 5. The rotor is designed for a prescribed enthalpy rise. The saved geometry of that rotor is then used in off-design assemblies. Each off-design assembly has the inflow as defined from the results of the sector averaging as shown in Fig. 4. The losses of these sectors are computed and mass averaged to get the overall rotor loss. It is argued here that the rotor designed in this fashion does not necessarily lead to minimal losses although it is intuitive to treat the design point should as the average of the non-uniform flow field the rotor is supposed to operate under. The rationale being that the blade resulting from averaging the flow will minimize the fluctuations when operating in the true flow. Before the validity of this idea is established, an analysis of the composition of rotor losses is presented. For the purposes of this study, an empirical loss model based on the book by Aungier¹⁹ is used.

The design profile loss is an empirical correlation of loss with equivalent diffusion factor as shown in Eq.2. Further, the equivalent diffusion factor is a function of the design incidence (i^*), design deviation (δ^*), inlet and exit blade metal angles (κ_1, κ_2), solidity (σ), and axial velocity ratio ($\frac{C_{m1}}{C_{m2}}$) as shown in Eq.3.

$$\frac{\bar{\omega}^* \cos \beta_2^*}{2\sigma} \left(\frac{W_1^*}{W_2^*} \right) = f(D_{eq}^*) \quad (2)$$

$$D_{eq}^* = \left(\frac{W_{max}}{W_1} \right)^* \frac{W_1^*}{W_2^*} = f(i^*, \delta^*, \kappa_1, \kappa_2, \sigma, \frac{C_{m1}}{C_{m2}}) \quad (3)$$

Some corrections are also made for Mach number and for off-design incidence. A plot of the loss coefficient and incidence angle (in degrees) is shown in Fig. 7. It is evident that the loss is not a linear function of incidence (in fact, it even seems asymmetric about the vertical axis at the minimum loss point).

Ideally, the preference would be for all off-design points to operate at design incidence, so minimum losses can be achieved. However, since the flow field is not uniform, it is not possible for all off-design incidences to be equal to design incidence. An important insight can be gathered from Fig. 7. Had the losses been a linear function and of the same slope (magnitude) in either direction of the minimum loss point, the losses in the off-design conditions obtained from operating the blade designed for averaged flow would also be minimum. This is true because all circumferential sectors would contribute equally to the overall loss per unit mass flow. Because of the asymmetric and non-linear function of the loss models on either side of the minimum

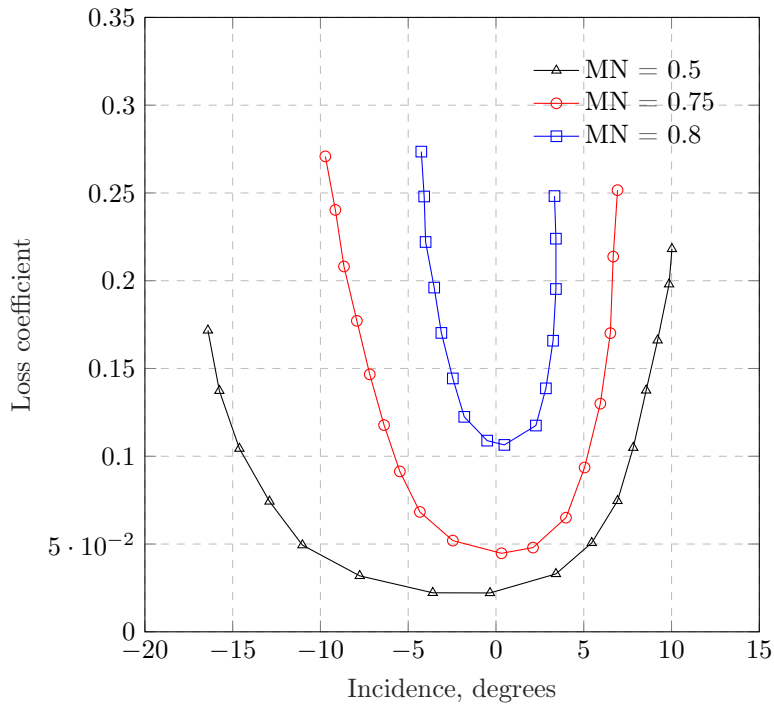


Figure 7. Variation of rotor loss coefficient with incidence angle, reproduced from Saravanamuttoo.²⁰

loss point, some circumferential sectors contribute more to the overall loss and minimizing the losses in those sectors is more important. It is hypothesized that when operating in a distorted flow field, minimum losses of the rotor does not always correspond to the rotor blade that is designed for a uniform flow obtained by averaging the distorted flow field condition.

Recalling that the design point is not a true operating point, two scalar parameters (sc_i and sc_δ) are introduced that modify the design incidence and deviation only in the design mode. The loss, it therefore, calculates in the design mode is not the correct form of the loss because its design incidence and deviation are not the correct ones. However, when operating in the off-design mode, sc_i and sc_δ will be set to unity so the losses computed in the off-design mode are correct. The idea is to create the optimal blade angles when operating in off-design mode. These scalars, sc_i and sc_δ , can be varied until the minimum loss is achieved when operating in the asymmetric flow field.

B. Unsteady rotor response

The time varying incidence angle on the fan blades as they rotate in the spatially non-uniform flow results in unsteadiness. The departure of the aerodynamic performance from quasi-steady performance depends on the per-rev distortion patterns, the extent of distortion, and finally the rate of incidence variation. The assumption that the fan blades respond to the incoming flow instantaneously is not necessarily true.

It is assumed that the distortion is steady state and that the losses are accounted for by quasi-steady calculations. Here in, the work by Carta²¹ is used. Fig. 8 summarizes the process. First, the quasi-steady performance of the rotor is computed. The flow properties at the rotor exit and inlet can be used to compute the axial and tangential forces. These forces can then be normalized and written in terms of coefficients of axial and tangential forces. The lift and drag coefficients can be obtained from force coefficients. The lift and drag coefficients of the rotor are then compared with the lift and drag coefficients of the airfoil and a relationship is obtained. The airfoil unsteady lift and drag are computed and the same relationship is used to obtain the rotor unsteady lift and drag coefficients. Reverse calculation is performed to backtrack the unsteady force coefficients, forces, and finally the unsteady flow parameters. Below, the description of all these steps are outlined.

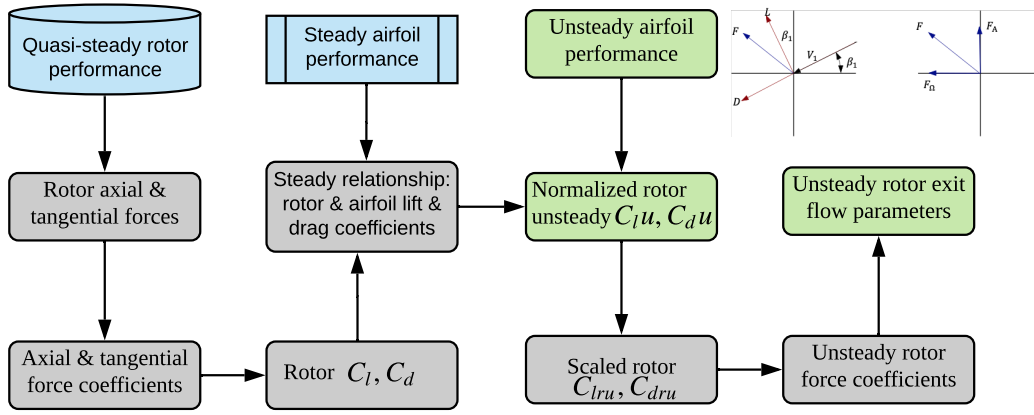


Figure 8. Unsteady approximation from quasisteady rotor performance.

Step 1: Quasi-steady rotor performance

The flow at the exit of Fig. 6 is the quasi-steady response of the rotor.

Step 2: Quasi-steady axial and tangential rotor forces

Consider a rotor rotating at an angular velocity, ω . The rotor is shown in Fig. 9 and is represented as a disk for simplicity. A fluid particle enters the rotor at a radius r_1 with absolute velocity V_1 , and exits the rotor at radius r_2 with absolute velocity V_2 . Here station 1 is the rotor inlet and station 2 is the rotor exit.

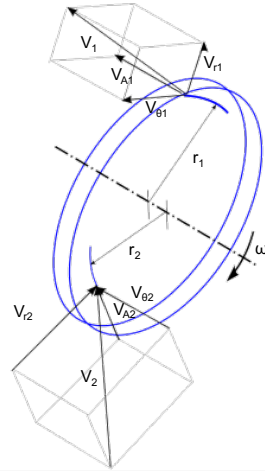


Figure 9. A rotor represented as a wheel.

The axial force provided by the rotor is the sum of the force due to change in axial momentum and change in static pressure across the rotor. Subscript A refers to the axial property. The axial force is given by Eq. 4, where F_{AH} refers to the axial force due to momentum change and F_{AP} refers to the axial force due to pressure change.

$$F_A = F_{AH} + F_{AP} \quad (4)$$

The axial force due to momentum change through a blade passage across a rotor is given by Eq. 5, where $\Delta\dot{m}$ refers to the mass flow through the blade passage and $A_{passage}$ is the blade passage area.

$$F_{AH} = \Delta\dot{m}_2 V_{A1} - \Delta\dot{m}_1 V_{A2} = A_{passage}(\rho_1 V_{A2}^2 - \rho_2 V_{A1}^2) \quad (5)$$

The axial force due to pressure difference is given by Eq. 6

$$F_{AP} = A_{\text{passage}}(p_2 - p_1) \quad (6)$$

From Eqns. 5 and 6, Eq. 4 can be written as:

$$F_A = A_{\text{passage}}(\rho_1 V_{A2}^2 - \rho_2 V_{A1}^2) + A_{\text{passage}}(p_2 - p_1) \quad (7)$$

Similarly, the tangential force can be computed by the change in the tangential momentum of the flow across the rotor, which is given by Eq. 8, where V_θ represents the swirl velocity.

$$F_\theta = \Delta \dot{m} V_{\theta 2} - \Delta \dot{m} V_{\theta 1} = A_{\text{passage}} V_A (\rho_1 V_{\theta 1} - \rho_2 V_{\theta 2}) \quad (8)$$

Step 3: Coefficients of axial and tangential forces

The axial and tangential forces computed in Step 2 can be written in terms of coefficients (Eqns. 9 and 10) by normalizing by the dynamic pressure at the rotor inlet and the reference area, which is taken as the product of blade span and the airfoil chord length.

$$C_{FA} = \frac{F_A}{\frac{1}{2} \rho V_1^2 A_{\text{passage}}} \quad (9)$$

$$C_{F\theta} = \frac{F_\theta}{\frac{1}{2} \rho V_1^2 A_{\text{passage}}} \quad (10)$$

Step 4: Conversion to lift and drag coefficients

The axial and tangential forces are represented in the vertical and horizontal axes in the right side of Fig. 10. The vectors (in red) on the left side represent lift and drag forces.

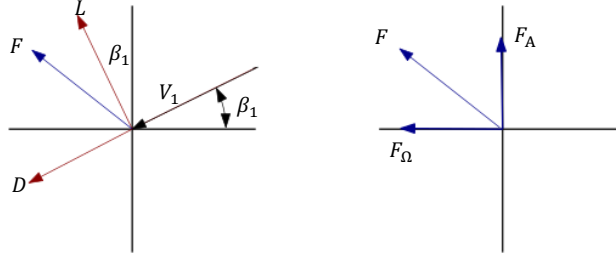


Figure 10. Relationship between axial-tangential forces to lift-drag forces.

Geometric relationships can be used to convert the axial and tangential forces to lift and drag forces in the forms shown in Eqns. 11 and 12.

$$L = F_A \cos \beta_1 + F_\theta \sin \beta_1 \quad (11)$$

$$D = -F_A \sin \beta_1 + F_\theta \cos \beta_1 \quad (12)$$

The same relationships can also be applied to the coefficients (shown in Eqns. 13 and 14)

$$C_L = C_{FA} \cos \beta_1 + C_{F\theta} \sin \beta_1 \quad (13)$$

$$C_D = -C_{FA} \sin \beta_1 + C_{F\theta} \cos \beta_1 \quad (14)$$

Step 5: Steady lift and drag of airfoil

To compute the steady lift characteristics, thin airfoil theory is utilized and is modified to account for camber and thickness. According to the thin airfoil theory, the lift slope is given by 2π . Experimentally, it has been observed that the lift curve slope is a function of thickness-to-chord (t/c) and is given by Eq. 15.²²

$$\frac{dc_l}{d\alpha} = 2\pi \frac{[1 + (0.77t/c)]}{[1 + (0.77t/c)^2]} \quad (15)$$

According to the thin airfoil theory, zero lift also occurs at zero degrees angle of attack. The zero lift angle of attack ($\alpha_{L=0}$) is a function of airfoil camber as shown in Eq.16.

$$\alpha_{L=0} = -2\theta_{\text{cam}} \quad (16)$$

From Eqns.15 and 16, the lift at any angle of attack can be written as

$$c_l = \frac{dc_l}{d\alpha}(\alpha - \alpha_{L=0}) \quad (17)$$

A steady drag model can be assumed at this point, since the purpose is to use the departure of unsteady characteristics from steady characteristics. To obtain the steady state drag values, Carta²¹ made some assumptions and their model was in good agreement with the experimental results for drag coefficients. Since the focus of this work is on the attached flow region, a constant value of c_d will be assumed.

Step 6: Scaling and relating rotor and airfoil lift and drag coefficients

From this point on, subscripts R and A will be used for rotor and airfoil respectively. Scaling laws are introduced so that the rotor and airfoil normalized coefficients overlap in the linear region of the lift curves. For the rotor, the linear region starts from the minimum loss point to the stall point. A normalized angle of attack scale for rotor can be written as shown in Eq. 18, where α_{RO} is the rotor minimum loss point, α_{RS} is the stall point, and α_R is rotor angle of attack. These angles of the rotor can be computed by running the rotor in the off-design mode up to the stall point and computing these angles using the velocity triangles at that point.

$$\sigma_R = \frac{\alpha_R - \alpha_{RO}}{\alpha_{RS} - \alpha_{RO}} \quad (18)$$

Similarly, Eq. 19 shows the scaling formula for the airfoil, where α_{AO} is the zero lift angle of attack, α_{RS} is the stall point, and α_a is airfoil angle of attack. Since potential flow theory is being used, stall angle will simply be assumed and the sensitivity of the results to the stall angle will be performed.

$$\sigma_a = \frac{\alpha_a - \alpha_{ao}}{\alpha_{as} - \alpha_{ao}} \quad (19)$$

Next, the lift coefficients for both rotor and airfoil follow the same scaling laws (Eqns. 20 and 21).

$$C_{LR}^* = \frac{C_{LR} - C_{LRo}}{C_{LRs} - C_{LRo}} \quad (20)$$

$$C_{La}^* = \frac{C_{La} - C_{Lao}}{C_{Las} - C_{Lao}} \quad (21)$$

The scaling laws above guarantee that the normalized steady lift coefficients of both rotor and airfoil coincide when plotted against the normalized angle of attack (σ). At stall point, both coefficients equal unity. So, the lift coefficients will likely not match after stall point (where $\sigma > 1$). However, for this work, only attached flow region will be considered. Based on this, a relationship can be constructed as shown in Eq. 22.

$$C_{LR}^* = C_{La}^* \quad (22)$$

For the drag coefficients, normalization is not performed, but a relationship between rotor and airfoil drag coefficients is established. These are, nevertheless, plotted against the stall parameter (σ) and the relation as shown in the form of Eq. 23 is established.

$$C_{DR} = C_{Da} + \delta_D \quad (23)$$

Step 7: Unsteady airfoil lift and drag coefficients

Experimental data for unsteady characteristics of any arbitrary shaped airfoil is not readily available. So, to model the unsteady lift, the use of Theodorsen's theory is made to predict the unsteady behavior of lift coefficient. At each circumferential location, the rotor inflow is given. With the information of the blade geometry in the off-design mode, the angle of attack for rotor blade can be calculated (Eq.24).

$$\alpha_R = f(\theta) \quad (24)$$

The rotor angle of attack can then be converted to corresponding airfoil angle of attack using the relationship from Eqns. 18 and 19. The relationship is shown in Eq. 25. All the parameters except airfoil angle of attack is known.

$$\frac{\alpha_R - \alpha_{Ro}}{\alpha_{Ro} - \alpha_{Ro}} = \frac{\alpha_a - \alpha_{ao}}{\alpha_{as} - \alpha_{ao}} \quad (25)$$

With the information of RPM, the airfoil angle of attack can be written as a function of time as

$$\alpha_a = f(\theta, RPM) = f(t) \quad (26)$$

The formulation can be written in terms of a sinusoidal function of mean angle of attack (α_m), amplitude (α_{amp}), frequency (ω), and phase (ϕ) as shown in Eq. 27.

$$\alpha_a(t) = \alpha_m + \alpha_{amp} \cdot \sin(\omega t + \phi) \quad (27)$$

It is now possible to compute the unsteady airfoil lift when pitching at some frequency. Theodorsen's theory can be used to compute the unsteady lift. This theory solves the equations on a frequency domain. Reduced frequency is used to compute the unsteady variation. The reduced frequency (k) is given by Eq. 28.

$$k = \frac{c/U}{2 \times \pi/\omega} \quad (28)$$

Theodorsen's function $C(k)$ is given by Eq. 29.

$$C(k) = \frac{\int_b^\infty \frac{\mu}{\sqrt{\mu^2-1}} e^{\iota k \mu} d\mu}{\int_b^\infty \sqrt{\frac{\mu+1}{\mu-1}} e^{\iota k \mu} d\mu} \quad (29)$$

This can further be written in terms of Hankel functions as shown in Eq. 30 and the phase is given by Eq. 31.

$$C(k) = \frac{H_1^{(2)}(k)}{H_1^{(2)}(k) + \iota H_0^{(2)}(k)} \quad (30)$$

$$\phi = |C(k)| \quad (31)$$

The resulting equation for unsteady lift coefficient is

$$c_{lau}(t) = -\frac{b}{U_\infty} [U_\infty \pi \dot{\alpha} - b \pi a \ddot{\alpha}] - \frac{2\pi}{U_\infty} C(k) [U_\infty \alpha(t) + b(\frac{1}{2} - a)\dot{\alpha}(t)] \quad (32)$$

Now that the unsteady hysteresis loop for the lift coefficient of the airfoil is available, the unsteady drag is computed in the similar way the steady drag was calculated from the steady lift. The deviation of the unsteady drag from a baseline point will be assumed to be proportional to the lift deviation. In case the unsteady lift is above the steady lift, the unsteady drag will be assumed to be below the steady drag and when the unsteady lift is lower than the steady lift, the unsteady drag will be located above the steady drag value.

$$c_{dau}(t) = c_{das} (1 - \frac{c_{lau} - c_{las}}{c_{las}}) \quad (33)$$

Step 8: Normalized rotor coefficients from unsteady airfoil coefficients

The unsteady properties will also have a subscript u to differentiate it from its steady counterpart. First, the unsteady airfoil coefficients are normalized using the same scaling used in Eq. 21, which is re-written for unsteady coefficient in Eq. 34.

$$C_{Lau}^* = \frac{C_{Lau} - C_{Lao}}{C_{Las} - C_{Lao}} \quad (34)$$

To convert the normalized unsteady airfoil coefficients into normalized rotor coefficients, an assumption here is that the relation developed for steady normalized lift coefficient (Eq. 22) also holds true for the unsteady relationship. With that, the normalized rotor lift coefficients can be extracted from Eq. 35.

$$C_{LRu}^* = C_{Lau}^* \quad (35)$$

Step 9: Rotor lift and drag coefficients

Eqns. 36 and 23 can be used to obtain the rotor lift and drag coefficients.

$$C_{LRu} = C_{LRu}^*(C_{LRs} - C_{LRo}) + C_{LRo} \quad (36)$$

The rotor lift coefficient computed above is a function of time. Once the unsteady coefficients are obtained as functions of time, they can be converted back to the function of circumferential location (θ) given the rotational speed.

Step 10: Unsteady axial and tangential rotor forces

The coefficients of unsteady lift and drag can be transformed into axial and tangential rotor force coefficients. These relationships can be obtained from the vector diagrams in Fig. 10 and represented in Eqns. 37 and 38.

$$C_{FAu} = C_{LRu} \cos \beta_1 - C_{DRu} \sin \beta_1 \quad (37)$$

$$C_{F\theta u} = C_{LRu} \sin \beta_1 + C_{DRu} \cos \beta_1 \quad (38)$$

The axial and tangential forces can be extracted from the coefficients as shown in Eqns. 39 and 40.

$$F_{Au} = \frac{1}{2} \rho V_1^2 A_{\text{passage}} C_{FAu} \quad (39)$$

$$F_{\theta u} = \frac{1}{2} \rho V_1^2 A_{\text{passage}} C_{F\theta u} \quad (40)$$

Step 11: Unsteady rotor exit parameters

The axial force computed from previous step can be split into axial force due to the momentum change and pressure change as given by Eq. 4. Since the force due to change in momentum depends upon axial velocity, continuity needs to be respected. That is why, any change in axial force due to unsteadiness affects only the tangential force field. The change in static pressure can then be computed as shown in Eq. 41

$$p_2 = p_1 + \frac{F_{Au}}{A_{\text{passage}}} \quad (41)$$

The total pressure can be calculated using steady Bernoulli's equation (42).

$$P_{02} = p_2 + \frac{1}{2} \rho_2 V_{02}^2 \quad (42)$$

The velocity triangle at the rotor exit yields the computation of absolute flow velocity at rotor exit (Eq. 43).

$$V_{02}^2 = V_{A2}^2 + (U - V_{\theta 2})^2 \quad (43)$$

Re-arranging the Euler turbomachinery equation, the exit tangential velocity can be computed from Eq. 44.

$$V_{\theta 2} = V_{\theta 1} - \frac{F_{\theta U}}{\rho_1 A_{\text{passage}} V_{A1}} \quad (44)$$

Eq. 41 - Eq. 44 yield a final expression for the total pressure at rotor exit, which is shown in Eq. 45.

$$P_{02} = p_2 + \frac{1}{2}\rho_2 \left[V_{A2}^2 + \left(U - V_{\theta 1} + \frac{F_{\theta U}}{\rho_1 A_{\text{passage}} V_{A1}} \right)^2 \right] \quad (45)$$

When the velocity, static and stagnation pressures are known, all other thermodynamic properties can be calculated from thermodynamic relationships. These rotor exit flow properties are the inputs to the stator row.

C. Non-axisymmetric stator design

The unsteady flow parameters from rotor exit are used to generate velocity triangles for stator quasi-steady performance calculations and corresponding design. The unsteady performance of the complete stage can then be calculated. Multi-point multi-meanline method is used for design of stators. Multi-point refers to each circumferential location in the same way the rotor was treated, except in this case, the equations for design and not off-design are solved - the philosophy being that the stator has to match to the incoming flow from rotor exit.

$$i - \delta = (\beta_1 - \beta_2) - (\kappa_1 - \kappa_2) \quad (46)$$

Eq. 46 shows the relationship between incidence (i), deviation (δ), flow angles (β), and blade metal angles (κ) at inlet (1) and exit (2). For a symmetric stator, $(\kappa_1 - \kappa_2)$ is constant at all locations around the circumference. If the flow is symmetric, $(\beta_1 - \beta_2)$ is also uniform. Therefore, it is possible to bring the incidence and deviation towards their design values, where minimum losses occur, at every location. However, if the flow is not symmetric, $(\beta_1 - \beta_2)$ is not uniform, so in order to bring the incidence and deviation to their design values along all circumferential locations, $(\kappa_1 - \kappa_2)$ need to be adjusted.

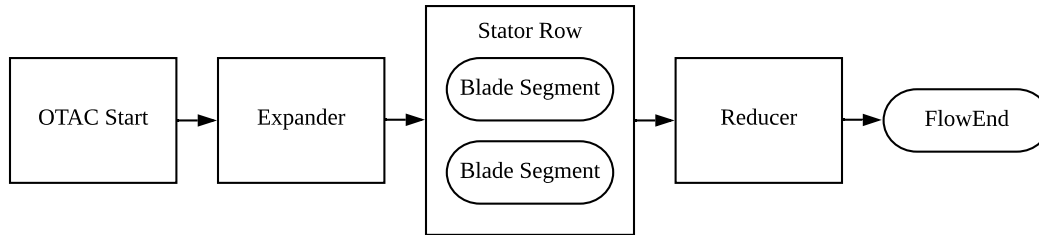


Figure 11. Schematic representing stator design assembly.

Fig. 11 shows the stator assembly for design point in the stator design process. There are as many points as there are circumferential sectors at the AIP. The schematic for the proposed approach is shown in Fig. 12. It can be seen that stator at rotor exit flow field is unsteady and non-uniform. The rationale is to design stator for the incoming flow at each circumferential sector's location. Unlike the rotor which was run in off-design mode, the stators are run in design mode since stators have to be designed to match rotor's exit flow.

D. Loop to converge on pressure rise across the stage

The determination of stator blade angles also provide stator exit flow information and thus, the stage performance. One might realize that the pressure rise across the stage at this point does not necessarily match the pressure rise a designer might have wished to achieve in the first place. The rotor designed in Fig. 6 is designed for a certain prescribed enthalpy rise. But, this prescribed rise in enthalpy in the rotor design point does not necessarily satisfy the pressure rise requirement across the stage. In order to meet that requirement, a Newton's solver is employed to vary that design enthalpy rise such that the actual stage pressure rise matches one that the designer wishes to achieve. The total pressure is computed using the ratio

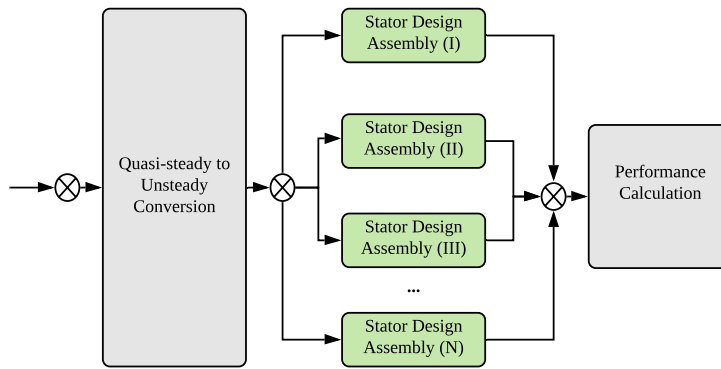


Figure 12. Stator design framework.

of mass averaged total pressure at the exit of the stator to the mass averaged total pressure at the rotor inlet. Fig. 13 summarizes the entire design framework.

At this point, it is important to note that the methodology outlined here does not consider any structural integrity analyses of the rotor blades that are operating in harsh conditions. The inclusion of these aspects along with the approach outlined here is discussed in a companion paper.²³

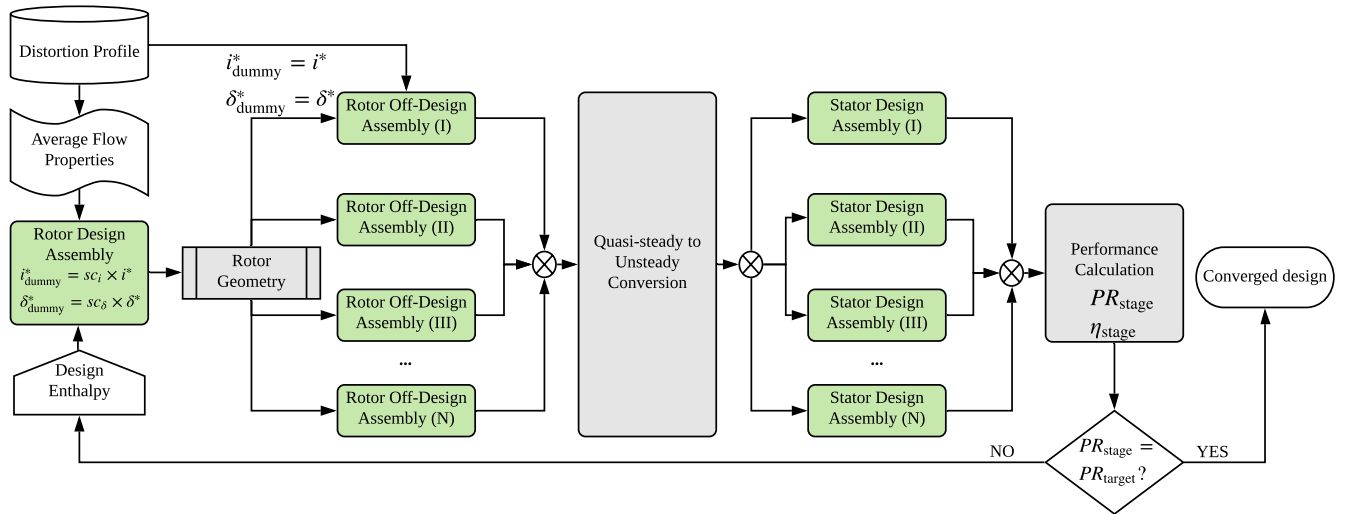


Figure 13. Fan stage design framework.

IV. Test Case Setup

For the purposes of this study, four different distortion cases will be considered - no distortion, low intensity distortion, mid intensity distortion, and high intensity distortion. The intensities are defined using total pressure distortion intensity ($dpcp$) given by Eq. 47, where PAV is the average total pressure on the annulus and PAVLOW is the average total pressure of the lower half of the total pressure profile.

$$dpcp = \frac{\Delta PC}{P} = \frac{PAV - PAVLOW}{PAV} \quad (47)$$

A sinusoidal function is used to generate the flow profiles at the AIP. Total pressure intensities of 0, 0.04, 0.078, and 0.12 are used as distortion input profiles, and they will be referred to as no distortion, low distortion, mid distortion, and high distortion cases respectively. No swirl is considered in these cases. Fig. 14 shows profiles of inlet total pressure, inlet mass flow, and inlet total temperature for the four cases. Total temperature and mass flow follow similar profiles as the total pressure for the test cases. Table 1 shows the requirements and design choices made for the initial set of test cases,

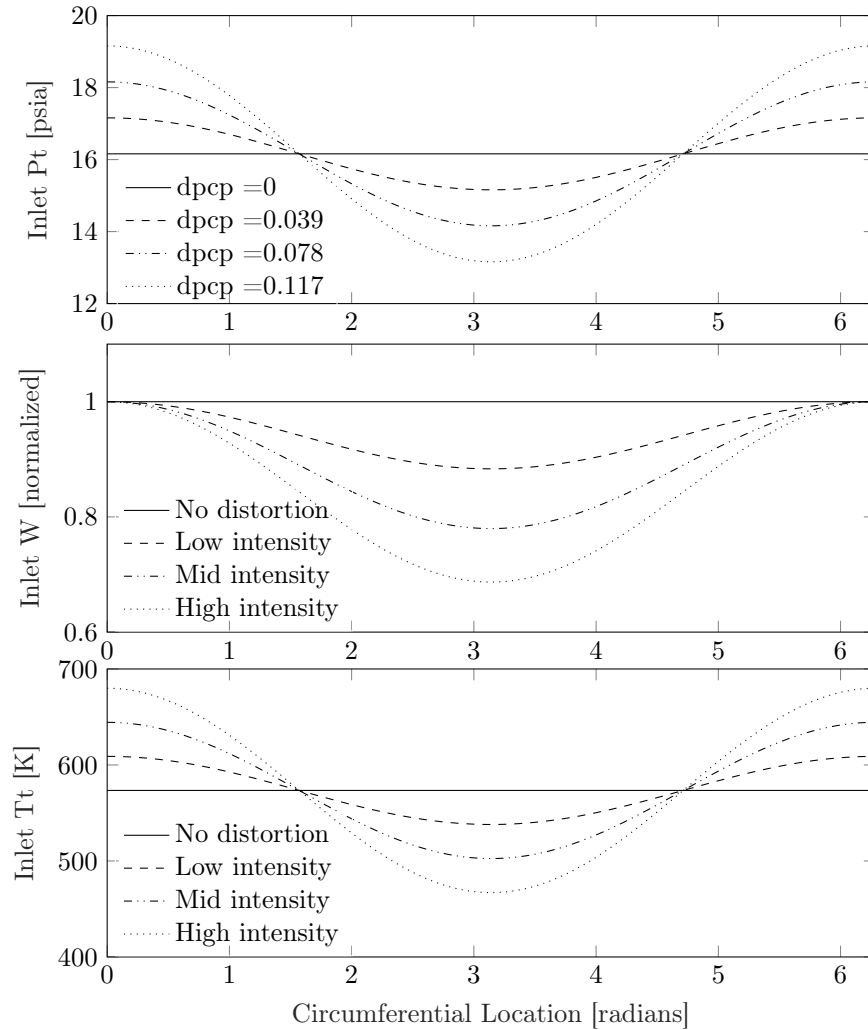


Figure 14. Flow profiles representing various distortion cases.

Table 1. Test case fan design parameters

Parameters	Values
Stage pressure rise requirement	1.25
RPM	4000
Tip radius	24"
Tip chord	7.2"
Taper type	No taper
Hub to tip ratio	0.25
Number of rotor blades	23
Number of stator blades	33
Stator chord	4.5"
Rotor airfoil type	Double circular arc
Machine type	Constant tip radius
Design type	Free vortex

V. Results

A. Optimization of rotor loss coefficients

As shown in Fig. 6, the incidence and deviation scalars (sc_i and sc_δ) vary the design incidence and deviation values, where a value of 1 corresponds to the true values. Table 2 shows the results of optimizing the rotor loss coefficients by using these scalars compared to the case when the rotor was designed for average operating flow without any other changes (i.e. scalars set to 1 everywhere). It can be seen that the loss coefficients are, indeed, lower when the scalars are changed. The reduction in the loss coefficients tend to be higher with increasing intensity of distortion, with the high distortion case observing a reduction in 1.2% of the loss coefficient.

Table 2. Effect of varying incidence and deviation scalars on rotor loss coefficients.

Case	Loss coefficient (i_{sc} and $\delta_{sc} = 1$)	Loss coefficient (optimal i_{sc} and δ_{sc})	Change
No distortion	0.0484	0.0484	0.00%
Low distortion	0.0498	0.0496	0.40%
Mid distortion	0.0533	0.0527	0.86%
High distortion	0.0587	0.0580	1.20%

The results of the low distortion case is discussed here. Fig. 15 shows the surface plot (left) of mass averaged loss coefficient as a function of incidence and deviation scalars. It is evident from the figure that the incidence scalar has a larger contribution to minimizing the overall rotor losses. This makes sense since the incidence angles also affect the losses in a larger proportion. Varying the deviation scalar does not follow the smooth trend as demonstrated by the incidence scalar, but it does contribute to further minimize the rotor losses (although a relatively smaller contribution). The exact behavior of these shapes depend on the loss models being used, so variants on these results can be expected with different loss curves. On the right side of Fig. 15, the contour plots of the coefficients are shown. While it is clear that the loss curves form a bucket shape, what is not intuitive is the location of the minimum loss. In the figure, [1,1] represent the design incidence and deviation of the blade (4° and 9° respectively, in this test case). If a blade was being designed, it would set the incidence angle for the design flow to be 4° . However, in Fig. 15 [right], the minimum losses occur when the scalars are at $[0.95, 0.4]$ ($i_{dummy}^* = 3.8^\circ$ and $\delta_{dummy}^* = 3.6^\circ$). These results also confirm the initially posed argument that when operating in distorted flow conditions, the minimum losses for the averaged flow are not necessarily near design values of incidence and deviation. Why this

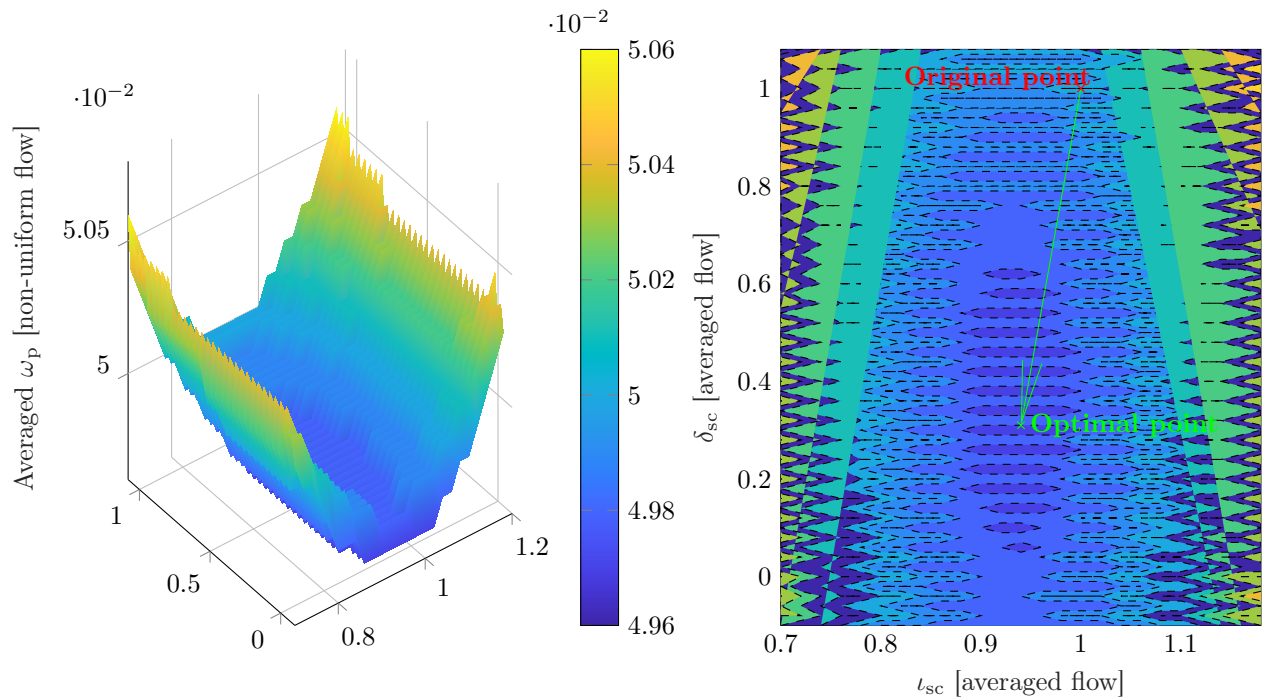


Figure 15. Rotor loss minimization: optimal incidence and deviation [surface plot: left; contour plot: right]

occurs is because of the non-linear nature of the loss curves (an example is the incidence curve shown in Fig. 7).

B. Loss coefficients: quasi-steady vs. unsteady rotor performance

The computation of unsteady rotor performance involves calculation of unsteady lift coefficient based on Theodorsen's theory. The results of the airfoil unsteady model is verified for a simple sinusoidal pitching condition ($\alpha = \alpha_0 + A_0 \sin(\omega t)$) where $\alpha_0 = 0^\circ$, $A_0 = 10^\circ$, and $k = \frac{c}{U_\infty} / \frac{2\pi}{\omega}$. The time varying lift coefficients of the airfoil is observed in Fig. 16. The results shown here exactly match with the pitching results shown by Gulcat.²⁴

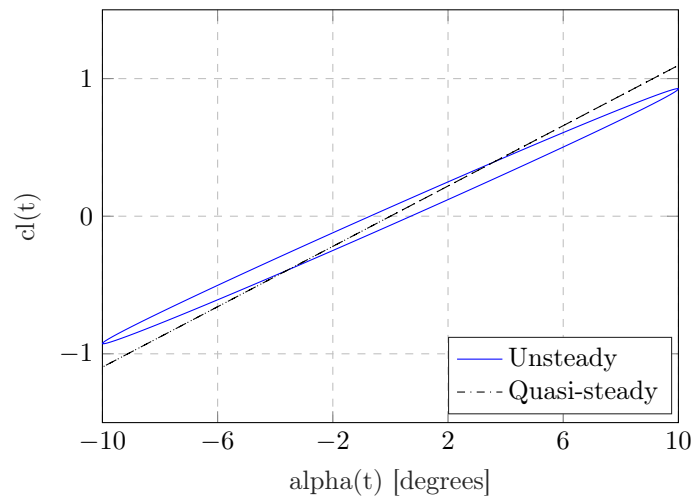


Figure 16. Quasi-steady and unsteady c_l of a thin airfoil pitching about 0° [amplitude = 10° , $k = 0.1$].

The effect of unsteady rotor response on rotor loss coefficients can be observed in Fig. 17. Note that when computing these losses, the rotor was not optimized for incidence and deviation. This is performed to only illustrate the effect of unsteadiness. In presence of no distortion, the results are the same. It makes sense because the rotor in relative reference does not experience any unsteadiness. At low level of distortion an increase of 0.2% in rotor loss is observed. The two curves (quasi-steady and unsteady response) tend to diverge at higher levels of distortion, with 1% difference for the high distortion case. Although the trends shall likely remain the same, the magnitudes will likely differ with changing geometries and flow profiles. The inclusion of unsteady effects also effects the flow downstream of the rotor, thereby affecting stator design. The overall effect of including unsteadiness modeling in the stage efficiency is explored later.

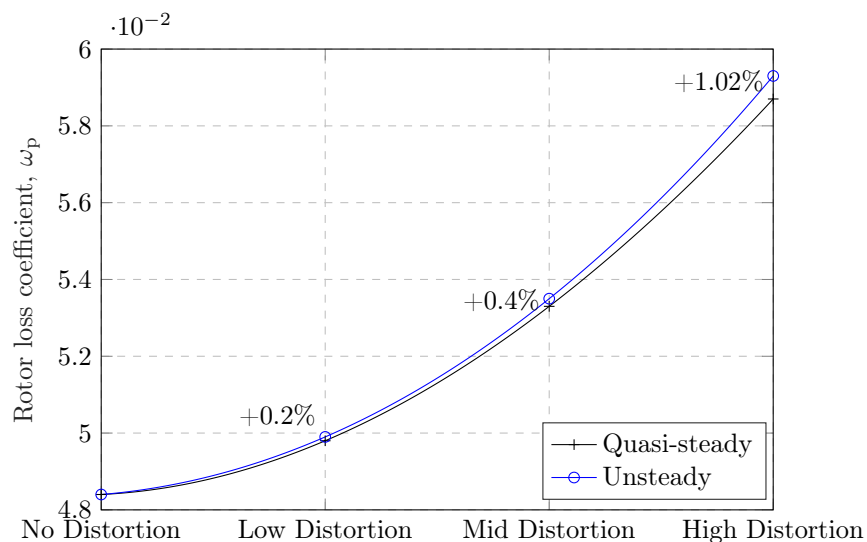


Figure 17. Effect of unsteady response on rotor loss coefficients.

C. Non-axisymmetric stator design

Fig. 18 shows the variation in the stator inlet blade metal angles for various distortion levels. As expected, the stators are symmetric in presence of no distortion. But, as the level of distortion increases, the level of variation seems to increase for both hub and casing. The proposed method can, hence, design stators with the degree of asymmetry established by the rotor exit flow.

Another observation is that the areas of high blade angles at the stator inlet correspond to the regions of low inlet mass flow and total pressure. Lower axial velocity increases the effective angle from the stator's perspective. This leads to higher angles for stators so the effective incidence is lowered. A third observation is the degree of symmetry of the curves about the 180° . It is interesting to note that the prescribed incoming flow was a pure sinusoidal function: i.e. it was symmetric about 180° . But, as the distortion intensity increases, the curves tend to be less symmetric. This can be attributed to the unsteady rotor response. The rotor exit flow is not just a function of the incoming flow at that location but also the history of the flow. It was seen that increasing distortion levels increases unsteadiness, and its effects can also be visualized in stator design. Therefore, unsteadiness not only effects the performance prediction for the rotor but effects the design downstream. A final observation is regarding the difference in graphs between the hub and the casing. The variation is higher in the casing region compared to the hub region: compare for the high intensity case, the variation of 30° to 45° for the hub region vs. 15° to 40° for the casing region. This implies that the effect of distortion is more pronounced in the tip region despite a uniform inflow for the sector. This rotor was designed on a free-vortex condition: equal enthalpy rise was enforced from the hub to the tip. Because of radial equilibrium, the tip region experienced a lower total pressure, and therefore the effect became more pronounced in tip regions, suggesting the need for investigations of the impact of loading type on the stage aerodynamic performance.

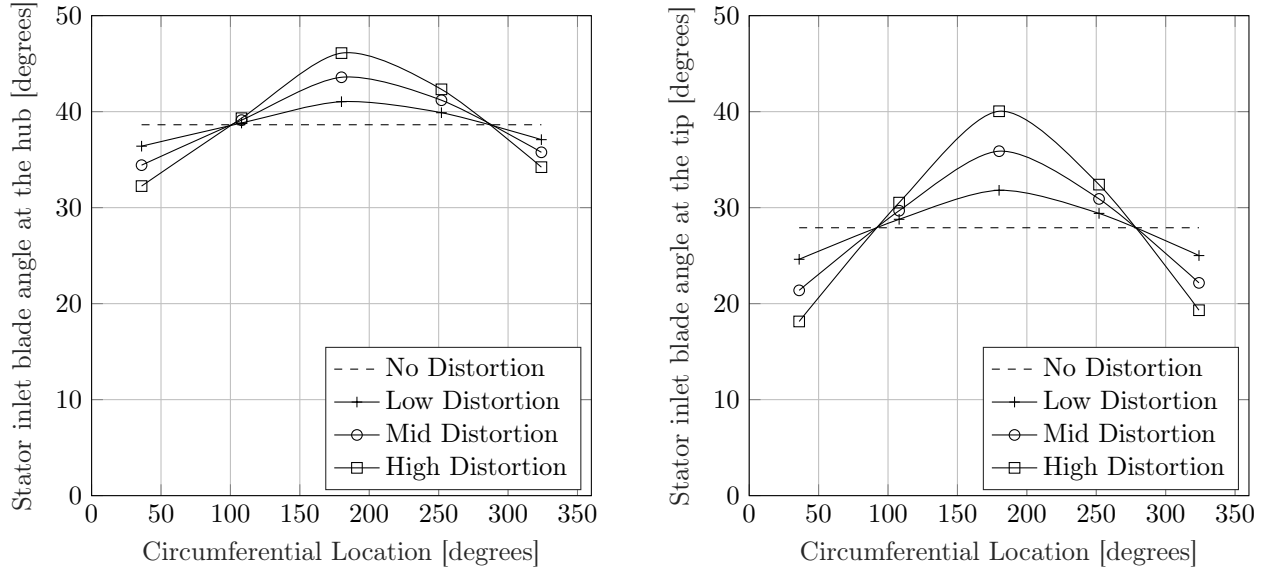


Figure 18. Circumferential variation of stator inlet blade angles [left: hub, right: casing].

D. Evaluation of the proposed framework

The results thus far dealt with specific components of the fan stage design. This section will evaluate the effect of each proposed changes on the overall stage efficiency. Isentropic rotor efficiency is given by Eq. 48, where ht_{2s} is the specific enthalpy of the flow at the exit for an isentropic process, ht_1 and ht_2 are the actual specific enthalpies of the flow at the inlet and the exit of the rotor.

$$\eta_r = \frac{ht_{2s} - ht_1}{ht_2 - ht_1} \quad (48)$$

Since specific enthalpies are extrinsic quantities, ht_1 and ht_2 are mass averaged. The isentropic enthalpy is calculated using the following process. First, the reference entropy at the inlet is calculated using the mass averaged total temperature and mass averaged total pressure based on the 'GasTb1' thermodynamic package. For an isentropic process, the entropy at the rotor exit is equal to the entropy at the rotor inlet. Finally, the exit enthalpy for an isentropic process is calculated by using the entropy and the mass averaged total pressure at the rotor exit. The functional relationships are given by Eqns. 49 - 51.

$$s_1 = f(Tt_1, Pt_1) \quad (49)$$

$$s_2 = s_1 \quad (50)$$

$$ht_{2s} = f(s_2, Pt_2); \quad (51)$$

Fig. 19 shows the effect of designing the fan stage with the framework presented here. The first point for all cases is the predicted efficiency if the fan were designed for the averaged uniform flow. Indeed, this is not the operating point, but if the fan were to operate in a uniform flow condition, this point represents the fan stage efficiency. All cases converge to approximately same stage efficiency (90.5%) because the averaged flows are almost identical. Any drop in efficiency can be compared to this point. When operating in distorted flow field, this fan experiences losses in both rotors and stators. It is evident that the drop in efficiency increases with increasing distortion intensity. The high distortion case experiences a drop of 5.86% in the stage efficiency. The length of the arrows represent the amount of this loss recovered using the framework presented here. The percents next to each point represent the efficiency recovered by the addition of that corresponding design element. Depending on the case, around 55-70% of this drop could be recovered through the design process.

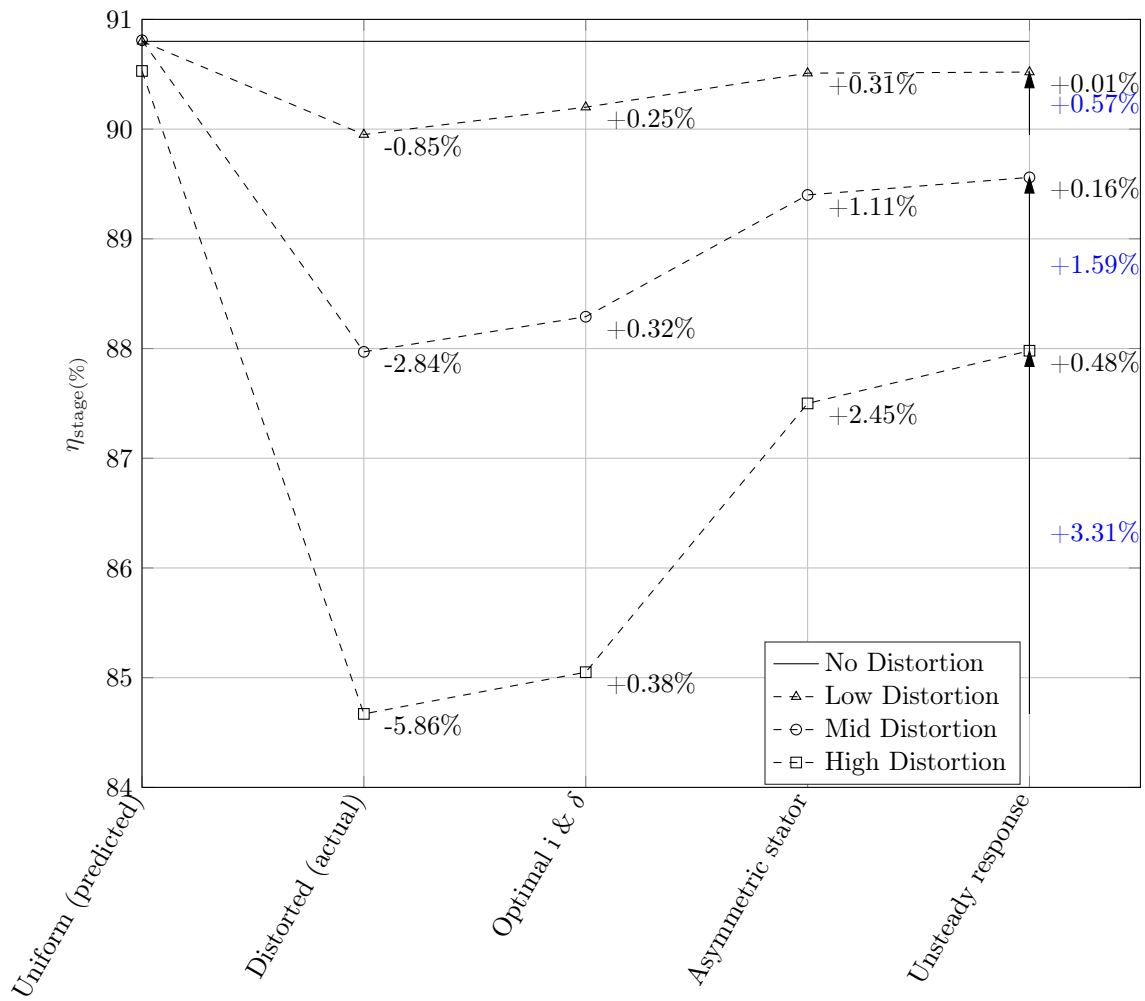


Figure 19. Impact of proposed design framework on stage efficiency for various distortion levels.

Table 3 shows the contribution of each design changes on total loss recovered. Optimization of incidence and deviation angles has a relatively stronger effect on low distortion cases. The contribution seems to weaken with the increasing distortion intensity. This is because the optimizer attempts to find the optimal values of incidence and deviation angles for minimal losses. It cannot change the incidence fluctuations present on the fan face. Since the fluctuations are higher for higher intensities, only a relatively smaller fraction of those losses can be recovered by optimizing the angles. Non-axisymmetric stators help recover the largest fraction of the losses as stator losses at each circumferential sector are minimized by varying the blade metal angles. Non-axisymmetric stator design changes are responsible for recovering 35-40% of lost efficiency, with higher recoveries corresponding to higher intensities. Increasing non-uniformities at the rotor inlet at higher intensities also equate to increasing non-uniformities at the rotor exit. Similarly, the unsteady effects start becoming more pronounced for higher intensities. Unsteadiness could be ignored at low distortion cases. At high distortion cases, however, the effect of including unsteadiness contributes to recovering more than 8% of overall losses (2% more than the contribution of optimizing incidence and deviation). The case for inclusion of any modeling capability is, therefore, justified depending on the type of distortion present.

Table 3. Contribution of various design changes on total loss recovered.

	Optimal i and δ	Asymmetric Stator	Unsteady Response	Total Loss Recovered
Low Distortion	29.40%	36.47%	1.15%	67.02%
Mid Distortion	11.26%	39.08%	5.63%	55.97%
High Distortion	6.48%	41.81%	8.19%	56.48%

E. Design space exploration

The results presented in Fig. 19 were evaluated on a fan stage with the high level design choices as defined in Table 1. Low computational cost associated with the method presented here allows for rapid exploration of design space in search of a better stage efficiency. Table 4 lists the chosen variables, their corresponding baseline, and lower and upper bounds.

Table 4. Bounds of variables for design space exploration.

Parameters	Baseline	Lower bound	Upper bound
Discrete variables			
Design type	Uniformly loaded	Hub loaded	Tip loaded
Taper type	1	1	3
Continuous variables			
Hub to tip ratio	0.25	0.23	0.3
Rotor tip chord	7.2"	6"	8.5"
Rotor exit area ratio	0.98	0.95	0.99
Stator exit area ratio	0.96	0.93	0.97
Stator chord	4.5"	3.5"	5"

Hub to tip ratio, rotor exit area ratio, and stator exit area ratio help to define the Mach number at the inlet and the exit of rotors and stators. Tip chord was used to control the solidity and the diffusion factor. Taper type of 1, 2, and 3 were defined with 1 representing no taper and 3 representing the 25% taper. Stator chord was used to control the stator efficiency. Three discrete loading types were defined: uniformly loaded, hub loaded, and tip loaded.

A total of 1000 cases were created using Latin Hypercube Sampling technique to design experiments. The rotor was subjected to the "mid distortion" case. Three radial segments were used in multi-meanline process. In addition, three metrics of interest were recorded: stage efficiency, diffusion factor at each segment at each circumferential location, and the reaction at the hub. The goal is to create a fan with maximum stage efficiency. The diffusion factor, defined in Eq. 52, is recorded. Any segment with diffusion factor greater than 0.6 is considered to be stalled. Hub reaction (Eq. 53) is recorded to ensure that negative reaction is not observed near the hub.

$$DF = 1 - \frac{V_{rel,2}}{V_{rel,1}} + \frac{|r_2 V_{\theta,2} - r_1 V_{\theta,1}|}{2\sigma V_{rel,1}(r_1 + r_2)/2} \quad (52)$$

$$R = \frac{h_2 - h_1}{ht_3 - ht_1} \quad (53)$$

1000 unique designs were designed on a standard desktop workstation with no parallel workers. All 1000 cases were run in less than three hours. The metrics of interest were recorded and a neural network model was formed using JMP[®], Version <15>. SAS Institute Inc. A single layer with three Hyperbolic tangent, two Linear, and three Gaussian nodes was able to provide a R^2 of greater than 0.97 for both training and validation data set. Stall limit was defined when the probability of any segment stalling was less than 0.01%. A two dimensional contour plot of stage efficiency with the presence of active stall limit constraint is shown in Fig. 20. Notice that the presence of stall limit constrained the solution to have a slightly lower stage

efficiency. An optimization was performed on the generated surrogate model. The optimum set of design variables was that increased the stage efficiency from 89.6% to 90.3%.

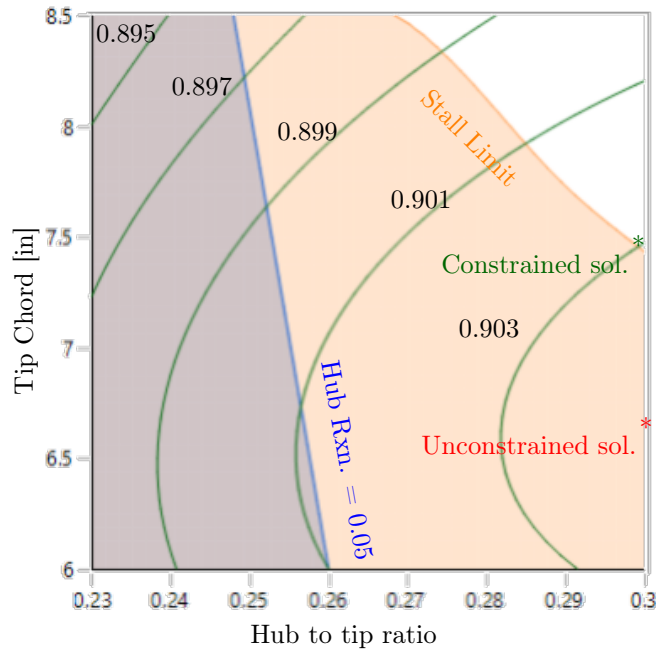


Figure 20. Contours of fan stage efficiency with constraints of stall limit and minimum hub reaction.

VI. Summary

A framework for conceptual design of a fan stage with non-axisymmetric stators in presence of distortion is presented here. Flow asymmetry was modeled using multiple circumferential sectors. Losses due to incidence variations were minimized by optimizing the incidence and deviation angles of rotor blades. The modification of quasi-steady rotor response to unsteady rotor response using simple analytical method helped to capture the unsteady effects. Non-axisymmetric stators in terms of blade metal angles were designed using multi-point multi-meanline method. It was observed that the tip region shows a higher degree of asymmetry. Non-axisymmetric stators helped to recover a large portion of distortion losses. Optimization of incidence and deviation angles were found to be more important for low distortion cases, while the effects of unsteadiness were recognized as important to be captured in higher distortion intensities. Depending on the distortion type, 55-70% of the losses were recovered. The computational time advantage afforded by the tools used in this framework also allowed for a wide range of design space exploration to further optimize the design while not violating any constraint. The approach presented here leverages and extends on to the already existing conceptual design tools, thereby making it a suitable method for conceptual design of a fan stage under distortion.

References

- ¹Cousins, W. T., Voytovych, D., Tillman, G., and Gray, E., “Design of a Distortion-Tolerant Fan for a Boundary-Layer Ingesting Embedded Engine Application,” *53rd AIAA/SAE/ASEE Joint Propulsion Conference*, 2017, p. 5042.
- ²Fowler, T., “Jet Engines and Propulsion Systems for Engineers,” *GE Aircraft Engines, USA*, 1989.
- ³Dean, R. C., “On the necessity of unsteady flow in fluid machines,” *Journal of Basic Engineering*, Vol. 81, No. 1, 1959, pp. 24–28.
- ⁴Cumpsty, N. A., *Compressor aerodynamics*, No. BOOK, Longman Scientific & Technical, 1989.
- ⁵Zierke, W. C., “Unsteady force calculations in turbomachinery,” Tech. rep., Pennsylvania State Univ University Park Applied Research Lab, 1991.
- ⁶Pearson, H. and McKenzie, A., “Wakes in axial compressors,” *The Aeronautical Journal*, Vol. 63, No. 583, 1959, pp. 415–416.
- ⁷Hawthorne, W., Mitchell, N., McCune, J., and Tan, C., “Nonaxisymmetric flow through annular actuator disks: Inlet distortion problem,” 1978.
- ⁸Cousins, W., “A theory for the prediction of compressor blade aerodynamic response,” *34th AIAA/ASME/SAE/ASEE Joint Propulsion Conference and Exhibit*, 1998, p. 3308.
- ⁹Carta, F. O., “An analysis of the stall flutter instability of helicopter rotor blades,” *Journal of the American Helicopter Society*, Vol. 12, No. 4, 1967, pp. 1–18.
- ¹⁰Bielawa, R., “Synthesized unsteady airfoil data with applications to stall flutter calculations,” *Proceedings of the 31st Annual Forum of the American Helicopter Society*, 1975, pp. 13–15.
- ¹¹Leishman, J. G., “Challenges in modelling the unsteady aerodynamics of wind turbines,” *Wind Energy: An International Journal for Progress and Applications in Wind Power Conversion Technology*, Vol. 5, No. 2-3, 2002, pp. 85–132.
- ¹²Hall, D., Greitzer, E., and Tan, C., “Analysis of fan stage conceptual design attributes for boundary layer ingestion,” *Journal of Turbomachinery*, Vol. 139, No. 7, 2017, pp. 071012.
- ¹³Gunn, E. J. and Hall, C. A., “Nonaxisymmetric Stator Design for Boundary Layer Ingesting Fans,” *Journal of Turbomachinery*, Vol. 141, No. 7, 2019, pp. 071010.
- ¹⁴Jones, S. M., “Development of an object-oriented turbomachinery analysis code within the npss framework,” 2014.
- ¹⁵Ainley, D. and Mathieson, G. C., “A method of performance estimation for axial-flow turbines,” Tech. rep., Aeronautical Research Council London (United Kingdom), 1951.
- ¹⁶Dunham, J. and Came, P., “Improvements to the Ainley-Mathieson method of turbine performance prediction,” *Journal of Engineering for Power*, Vol. 92, No. 3, 1970, pp. 252–256.
- ¹⁷Kacker, S. and Okapuu, U., “A mean line prediction method for axial flow turbine efficiency,” *Journal of engineering for power*, Vol. 104, No. 1, 1982, pp. 111–119.
- ¹⁸Craig, H. and Cox, H., “Performance estimation of axial flow turbines,” *Proceedings of the Institution of Mechanical Engineers*, Vol. 185, No. 1, 1970, pp. 407–424.
- ¹⁹Aungier, R. H. and Cassin, I., “Axial-flow compressors: A strategy for aerodynamic design and analysis,” 2003.
- ²⁰Saravanamuttoo, H. I., Rogers, G. F. C., and Cohen, H., *Gas turbine theory*, Pearson Education, 2001.
- ²¹Carta, F. O., “Analysis of Unsteady Aerodynamic Effects on an Axial-Flow Compressor Stage with Distorted Inflow,” Tech. rep., Purdue Univ Lafayette in Project Squid Headquarters, 1972.
- ²²Pope, A., “On Airfoil Theory and Experiment,” *Journal of the Aeronautical Sciences*, Vol. 15, No. 7, 1948, pp. 407–410.
- ²³Pokhrel, M., Sarojini, D., and Mavris, D. N., “Conceptual level optimization of a fan stage under distortion considering aero-structural constraints,” *AIAA Aviation 2020 Forum*, 2020.
- ²⁴Gülçat, Ü., *Fundamentals of modern unsteady aerodynamics*, Springer, 2010.